Geomechanics and Engineering, *Vol. 35, No. 3 (2023) 221-239*
https://doi.org/10.12989/gae.2023.35.3.221

Study on the root interaction characteristics and nonlinear deformation prediction of root piles

Jilu Zhang[1,2a], Xiaohan Zhou*[1,2], Xuefeng Huang[3,4], Xinrong Liu[1,2], Jun Yuan[5], Xuelan Liang[6] and Juan Li[7]

[1]*School of Civil Engineering, Chongqing University, Chongqing 400045, China*
[2]*National Joint Engineering Research Center of Geohazards Prevention in The Reservoir Areas (Chongqing), Chongqing 400045, China*
[3]*School of Civil Engineering, Lanzhou University of Technology, Lanzhou, 730050, China*
[4]*Department of Military Installations Engineering, Army Logistical University of PLA, Chongqing 401311, China*
[5]*Northwest Electric Power Design Institute Co., Ltd. of China Power Engineering Consulting Group, Xi'an 710075, China*
[6]*Construction Branch of State Grid Qinghai Electric Power Company, Xining, 810001, China*
[7]*Qinghai Power Transmission and Transfer Engineering Co. Ltd., Xining, 810000, China*

(*Received December 24, 2022, Revised August 5, 2023, Accepted September 27, 2023*)

Abstract. As a new type of pile foundation, root piles have attracted more attention in the uplift design especially because of their unique structure. In this paper, based on the field tests the bearing capacity and load transfer law of straight pile, belled pile and roots pile were analysed. Results found the setting of multiple layers of roots along the pile depth can make the root resistance and skin friction resistance work simultaneously which improve the uplift resistance greatly. By using the numerical simulation tool, the uplift resistance of pile is analysed under the influence of different root length, density (number of roots) and spacing. It is found that increasing the root length and spacing can effectively improve the uplift resistance of the pile. However, the effect of increasing the spacing of roots is more significant. With increasing the roots density, the interaction development process between roots will assume to four main stages: stage I no interaction, stage II weak interaction, stage III strong interaction and stage IV strengthen. When the roots density is at stage II, there will be a high uplift resistance in addition to a little interaction. Finally, based on the load transfer method, a nonlinear deformation calculation method for the roots pile under uplift load were established. This method not only considered the influence of different stress conditions and roots positions on load distribution of roots, but also consider the influence of roots interaction at same layer and between layers on the uplift resistance.

Keywords: field test; nonlinear deformation; numerical simulation; root pile; uplift

1. Introduction

Tension piles are widely used in high-voltage transmission towers, anti-floating buildings and underground buildings. For traditional tension piles, the foundation uplift resistance can only be improved by increasing the diameter, length and number of piles. The use of traditional tension piles not only has certain requirements for the soil bearing capacity and construction space but also causes considerable waste of materials (Rattley *et al.* 2008, Wang *et al.* 2022, Moayedi and Mosallanezhad 2017).

Particulary, in the construction of high-voltage transmission towers, because the tower is often built in various complex geological structures and the construction space is limited, traditional tension piles cannot meet construction needs.

Based on the principle of bionics, a prefabricated root can be implanted into the soil around a pile body to simulate the anchoring effect of plant roots so that the foundation can meet the needs of a greater uplift resistance.

As a new type of pile foundation, root piles have been applied and studied as pressure-bearing foundations since their inception (Cui *et al.* 2021, Luo *et al.* 2022, Ding *et al.* 2017) and have been successfully applied to the Ma'anshan and Chizhou Yangtze River Bridges. Based on field measurements of the Ma'anshan Yangtze River Bridge. Huang *et al.* (2011) proposed a prediction and calculation method for the compressive deformation of root caisson foundations based on the Winkler model. However, the unique structural form of root piles also has great application and research value for uplift. Zhou *et al.* (2021) explored the uplift bearing characteristics of root piles under complex loads through field tests of combined horizontal and vertical loading and analysed the influence of the designing parameters such as pile length and diameter on the uplift resistance of foundations through numerical simulation. However, there are many factors affecting the uplift resistance of the roots, such as the design parameters of the roots, the load form and the strength of the soil; Additionally, the interaction between roots will affect the uplift resistance of the foundation. The research on the uplift bearing characteristics of root piles is

*Corresponding author, Associate Professor
E-mail: cqzhouxhan@126.com
[a]Ph.D. Student
E-mail: 540726390@qq.com

ISSN: 2005-307X (Print), 2092-6219 (Online)

Table 1 Physical and mechanical parameters of the soil

Number	Name	Depth h_i/(m)	Density ρ/(g·cm^{-3})	Void ratio e	Cohesion c/kPa	Internal friction angle φ/°
①	Silt	0~2	1.35	1.187	23	19.6
②	Silty clay	2~3	1.53	0.922	25	18.3
③	Silt	3~5	1.48	1.019	23	19.4
④	Silty clay	5~6	1.61	0.922	21	20.4
⑤	Silt	6~7	1.55	1	20	21.2
⑥	Silty clay	7~8	1.65	0.831	24	18.8
⑦	Silt	8~9	1.52	0.971	23	19.3
⑧	Silty clay	9~20	1.62	0.856	24	18.8

not comprehensive and cannot guide the uplift design of root piles. Moreover, there is no report related to the theoretical research on the prediction of uplift deformation of root piles, and the lag of theoretical research also limits the further application and popularization of root piles to a certain extent.

At present, the prediction and analysis methods of foundation deformation under vertical loads mainly include the load transfer method, shear displacement method and elastic theory method (Seed and Reese 1957, Cook *et al.* 1979, D 'Appolonia and Romualdi 1963). The shear displacement method is mainly applicable to small deformation conditions. The elastic theory method does not consider the continuity of the soil. Moreover, the elastic theory method is performed under the condition of foundation compression. In the calculation, it is assumed that the soil is an elastic semi-infinite body, while the soil in the process of foundation uplift is no longer considered an elastic semi-infinite body, and its nonlinear displacement is more obvious than that under compression. Regarding the load transfer method, the hyperbolic function model of load transfer was originally proposed by Seed and Reese through actual measurement. This method divides the pile into several sections, which are independent calculation elements, and the pile displacement is obtained by accumulating the calculation value of each element. Although the load transfer method also assumes the compression condition of pile foundations, it has been widely used in the deformation calculation of various pile foundations after continuous improvement and correction (Boonyatee and Lai 2020, Dias and Bezuijen 2018, Fan 2007). At present, the load transfer method is widely used in the deformation analysis of straight piles. For the special-shaped pile, the load transfer mechanism is more complex due to the sudden change in axial force at the position of the variable section. Therefore, the application of the load transfer method in special-shaped piles is also one of the hot topics in recent years (Liu *et al*. 2019; Chalmovsky and Mica 2020, AbdelSalam *et al.* 2014). For the roots pile, the installation of the roots layer not only increases the skin friction resistance but also greatly increases the end resistance. The pile body's stress mode differs noticeably from the conventional pile foundation (straight pile and belled pile). However, the load distribution mechanism of multi-layer roots in the process of loading is still unclear, more research is needed to better understand this process.

Although some researchers have studied the theoretical model of the roots pile deformation, the research findings have primarily focused on the compression of the foundation; no pertinent research on the foundation uplift has been discovered. Additionally, the theoretical prediction models in the current usage do not take into consideration the interaction process between roots (Cui *et al.* 2021, Luo *et al.* 2022, Ding *et al.* 2017).

Based on the gap of the previous research, this paper compares the variation laws of the uplift resistance of root piles, belled piles and straight piles through field tests and clear the characteristics of the uplift load transfer of root piles. Through numerical simulation, the influence characteristics of root interactions on the uplift resistance with different root lengths and spacing and root densities (number of roots) were analysed and load distribution model of roots were established. Based on the load transfer method, a nonlinear deformation calculation method for piles is established considering the interaction of roots, which is verified by field experiments and numerical simulations. The results can provide a reference and guidance for the uplift design and deformation prediction of root piles

2. Field test overview

2.1 Geological overview

The field test is performed in a loess area in Lanzhou, China, as shown in Fig. 1. The on-site soil layers are mainly composed of silt and silty clay; miscellaneous fill was observed within 2 m of the surface thickness, with relatively weak mechanical properties, and the rest of the layers are undisturbed loess. The underground water level is far lower than the elevation of the pile bottom, thus, the influence of water on the bearing capacity of the pile is ignored. The physical and mechanical parameters of the soil are shown in Table 1.

2.2 Test scheme and site layout

In this paper, the uplift tests were carried out on three different types of piles: straight piles, belled piles and root piles. The length of the buried part of the pile is 10 m, and the diameter is 1.2 m. The diameter of the belled base of the

Fig. 1 Geological conditions and test overview

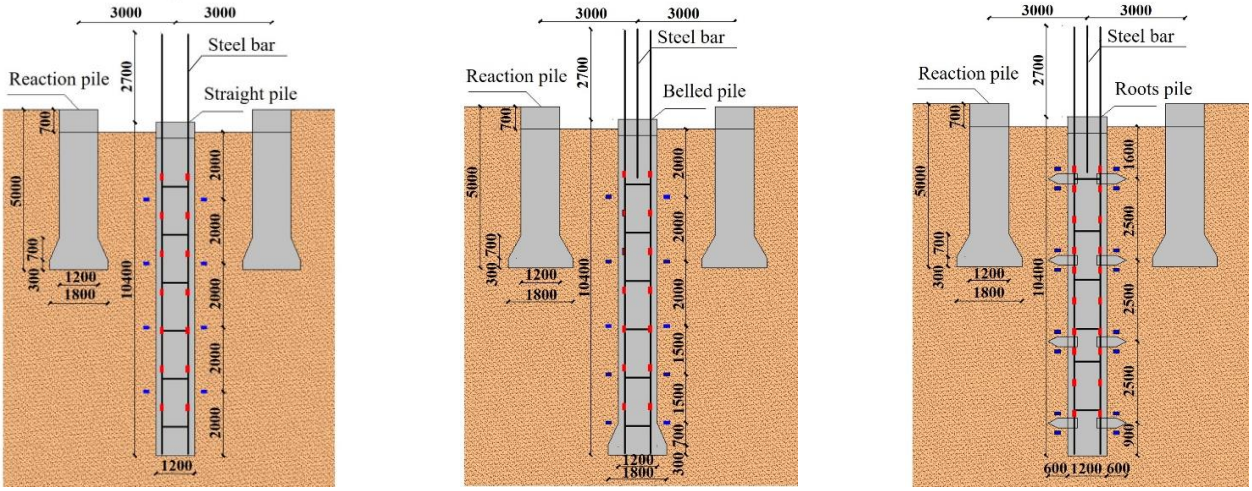

(a) Straight pile (b) Belled pile (c) Roots pile

Fig. 2 Profiles of the test piles (The blue mark indicates the vertical earth pressure sensor, and the red mark indicates the reinforcement stress meter)

belled pile is 1.8 m, and the height is 1 m. A total of 4 layers of roots are set for the root pile, with 6 keys in each layer (the buried part of each root is 0.6 m long, 0.3 m high and 0.15 m thick). The reaction piles, which are belled piles, is symmetrically arranged at 3 m from both sides of each test pile. The length of pile in the soil is 5 m, the diameters of the pile body and the belled base are 1.2 m and 1.8 m, respectively, and the height of the belled base is 1 m. To eliminate the influence of the pile group effect between test piles on the test results, the spacing of each group of test piles should not be less than 8 m, and the site layout is shown in Fig. 2.

The piles used in the field test are all manually excavated piles, and the concrete grade of the test pile is C40. Among them, the construction process of the root piles has been done as the following: root production - manual excavation - root installation - pouring piles, as shown in Fig. 3. It is worth noting that before installing the roots, manual excavation of guide holes is required. In order to ensure the bearing effect after the installation of the roots, the size of the guide holes is slightly smaller than the size of the roots. When the roots are inserted, the surrounding soil is compacted through the effect of expansion, thereby reducing the construction disturbance. The installation of the roots requires the use of a jack to simultaneously install the two symmetrical roots until the rooting depth reaches the design requirements. Before pouring the pile body, the concrete that sets in the pile body needs to be roughened to ensure effective connection between the roots and the pile body.

The testing adopts the slow load method for the loading process. According to the Technical Code of Testing Building Foundation Piles of China (JGJ 106-2014 2014), the standard to judge the failure of pile is as the following:

(1) Under a certain level of load, the displacement increment of pile top caused by this level of load is 5 times greater than that under the previous level of uplift load.

(2) The cumulative displacement of pile top exceeds 100 mm.

The ultimate uplift resistance of the straight pile has been estimated according to Eq. (1) and equal to 30t. Taking the ultimate uplift resistance of a straight pile as the benchmark, the loading amount of each stage is taken as about 1/10 of its limit value, i.e., 30 t. During the test, the straight pile is loaded to failure, while the belled pile and root pile are only loaded to the same load as the straight pile due to other test plans (JGJ 94-2008 2008).

$$Q_{ult} = H\pi dq_{sik} \tag{1}$$

where Q_{ult} is the ultimate uplift resistance of the foundation, H is length of the pile, d is the diameter, and q_{sik} is the ultimate skin friction resistance, which is generally 75 kPa for loess in the Lanzhou area.

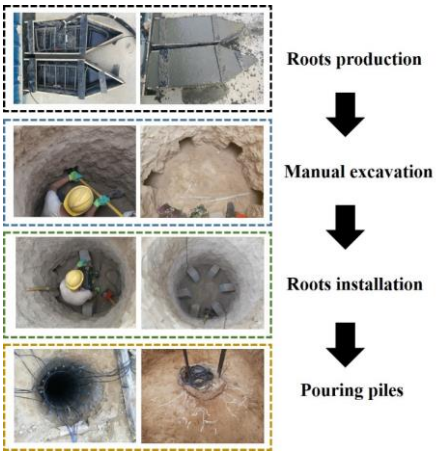

Fig. 3 Construction steps of roots pile

2.3 Loading and testing system

The loading system is mainly composed of a reaction pile, reaction beam, jack and steel bar. The operation steps of the loading system has been done according to the following order: 1) place the reaction beam on the top of the reaction pile on both sides of the test pile; 2) place the jack on the upper part of the reaction beam and ensure that the jack is perpendicular to the centre of the test pile; 3) fix the upper part of the jack with a steel bar through the cushion block and anchor bolt; 4) start the jacking procedures and load the tested pile. The field test layout is shown in Fig. 4.

The components of the test system is composed of a displacement meter, reinforcement stress meter and earth pressure sensor. Among them, 4 displacement meters are evenly arranged on the pile top, and the final displacement is the average result of the 4 displacement meters. The reinforcement stress meter is bound with the main reinforcement of the tested pile by welding. Each design position included two pieces symmetrically. The earth pressure sensor is placed 0.3 m from the pile body symmetrically through manual hole cutting according to the test requirements. The specific location information is shown in Fig. 2.

3. Field test results and analysis

3.1 Variation law of uplift resistance

Fig. 5 shows the field test load displacement curve of the straight pile, belled pile and root pile. For the straight pile, the curve development mode reflects a "sudden change", and its ultimate load is 2700 kN, while the belled pile and root pile show a "gradual change". When the load reaches 3000 kN, there is no obvious failure characteristics.

The development of the displacement for the straight pile can be divided into three stages: when $Q \leq 900$ kN, the pile is in the linear growth stage of elastic deformation; when 900 kN $\leq Q \leq$ 2700 kN, the pile is in the nonlinear growth stage of elastic-plastic deformation; and when Q $\geq$ 2700 kN, the pile is in the stage of rapid failure. Under the test load, the displacement development stages of the belled

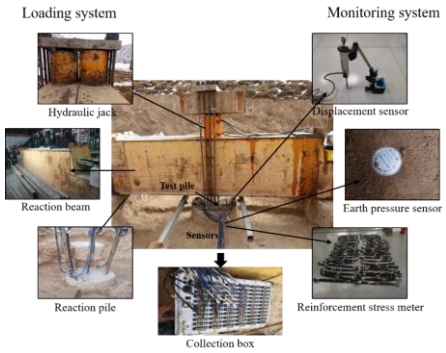

Fig. 4 Loading and monitoring system

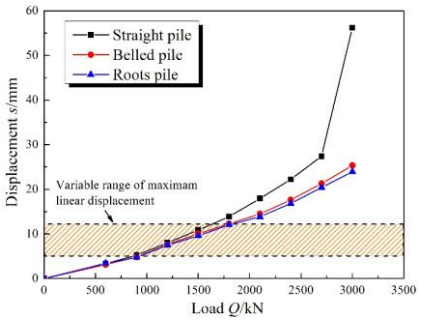

Fig. 5 Q-S curve of piles

pile and root pile mainly include the following stages: when $Q \leq 1800$ kN, the pile is in the linear growth stage; when $Q \geq 1800$ kN, the pile is in the initial stage of nonlinear growth. At this stage, although there is a nonlinear deformation trend, the increment is still small. In addition, with making comparison with the linear elastic development stage of the straight pile, the displacement of the belled pile and root pile increases approximately 240%, and the displacement of the two piles under the maximum test load is 45% and 42.6% that of the straight pile, respectively. This shows that the setting of the variable section significantly prolongs the linear elastic development stage of the pile under load and inhibits the generation of large deformation in the early stage and that the setting of multilayer roots has a more obvious inhibitory effect on displacement than the belled pile.

3.2 Axial force distribution of the pile

Fig. 6 shows the axial force distribution curves of the tested piles under different loads. The axial force of the three piles decreases with increasing depth. When the load of the belled pile is small, the axial force of the upper part of the pile body decreases rapidly. With increasing the loads value, the load of the belled base increases slightly compared with straight pile at the same position. When the load of the root pile is small, the axial force at the roots of the first and second layers shows a sudden drop. With increasing load, the roots of the third and fourth layers also gradually show an obvious sudden drop in axial force. This is because the bearing capacity of tension piles is primarily provided by the skin friction resistance and end resistance between the pile and the soil. When the pile is subjected to

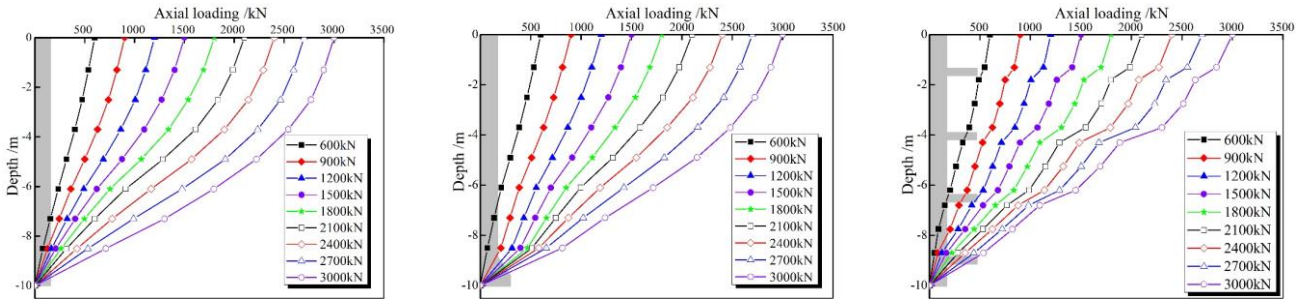

(a) Straight pile (b) Belled pile (c) Roots pile

Fig. 6 Distribution curve of axial force

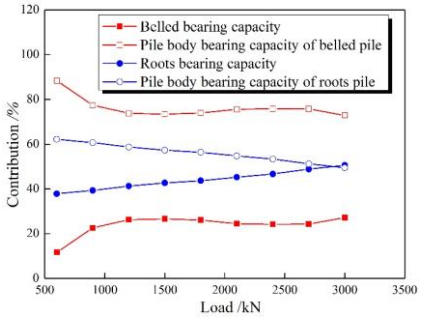

Fig. 7 Contributions of the uplift resistance of the protruding section and the pile body under different loads

the uplift load, the pile undergoes upward deformation, and the relative displacement between the pile and the soil generates skin friction resistance and end resistance in the soil, which leads to reduce the axial force along the longitudinal depth of the pile gradually. When the load is relatively small, the deformation of is mainly concentrated in the upper part of the pile, so the skin friction resistance of the upper soil is first exerted, as shown in the graph by the significant decrease in axial force in the upper part of the pile. The bearing behavior of root piles is similar to that of belled piles and straight piles. When the load is relatively low, the roots in the upper part of the pile first bear the load due to pile deformation. However, the uplift resistance of the roots is better than the straight part because of the end resistance, resulting a sudden change in the axial force at the position of the root. With the increase in load, the bearing capacity of the upper soil gradually reaches its limit, and the displacement of the pile gradually develops downwards. At this stage, the bearing capacity of the deeper soil begins to significantly exert, and the axial force at the position of the bell and the roots in the lower part of the pile undergoes significant increases.

The contributions of the uplift resistance of the protruding section and the pile body under different loads are shown in Fig. 7. The uplift resistance provided by the belled base and roots generally shows an upwards trend with load increasing, in which the belled base accounts for 11.7% and 27.2% of the total uplift resistance at 600 kN and 3000 kN, respectively. Roots account for 37.8% and 50.5% of the total uplift resistance at 600 kN and 3000 kN, respectively. Within the test load range, the uplift resistance of the belled base is always lower than that of the roots under the same load. When the value of the applied loads is small, the uplift resistance of the belled base is also small, and the resistance of the belled base lags behind the pile body, which is consistent with the existing research conclusions (Yu *et al*. 2020, Kong *et al*. 2013, Qian *et al*. 2019). At the initial stage of loading, the root uplift resistance is obvious, and the contribution of the root uplift resistance to the total uplift resistance increases almost linearly with increasing the applying loads. This shows that the bearing capacities of the roots and pile body are activated simultaneously, and the multilayer root setting ensures the stability against the uplift resistance of the pile and makes the soil at different depths bear the force together.

3.3 Skin friction resistance

Fig. 8 shows the distribution curves of the skin friction resistances of the tested piles. For comparison, the uplift resistance at the variable section is converted to the equivalent skin friction resistance. The skin friction resistance at the roots can be calculated by Eq. (2), while the equivalent skin friction resistance at the belled base can be obtained by Eq. (3).

$$q_i = \frac{Q_{i1} - Q_{i2}}{\pi d h_{Ri}} \tag{2}$$

where q_i is the root skin friction resistance at the ith layer. Q_{i1} is the axial force above the measuring point of the ith layer. Q_{i2} is the axial force below the measuring point of the ith layer. h_{Ri} is the distance between the upper and lower measuring points of axial force at the ith layer.

$$q_b = \frac{Q_b}{\pi d h_b} \tag{3}$$

where q_b is the skin friction resistance at the belled base, Q_b is the axial force at the measuring point at the belled base, and h_b is the height of the belled base.

The skin friction resistance at different positions of each pile increases with increasing the applied load before reaching the limit. However, the development laws of different types of pile are not the same. The skin friction resistance of the straight pile increases first and then decreases with depth. The position of the maximum value of the skin friction resistance gradually moves down from -6 m to -8.5 m with increasing load. When the load is small, the development law of the skin friction resistance of the belled pile is similar to that of the straight pile. The

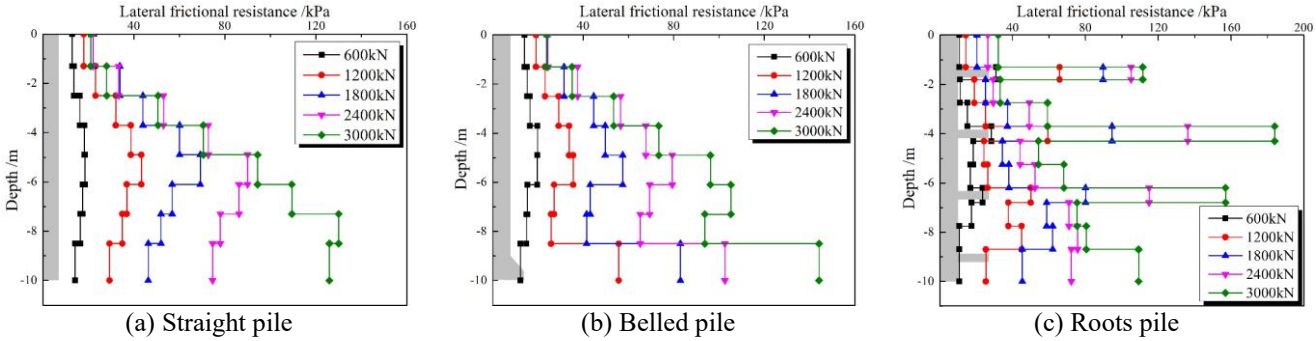

(a) Straight pile (b) Belled pile (c) Roots pile

Fig. 8 Distribution curve of the skin friction resistance

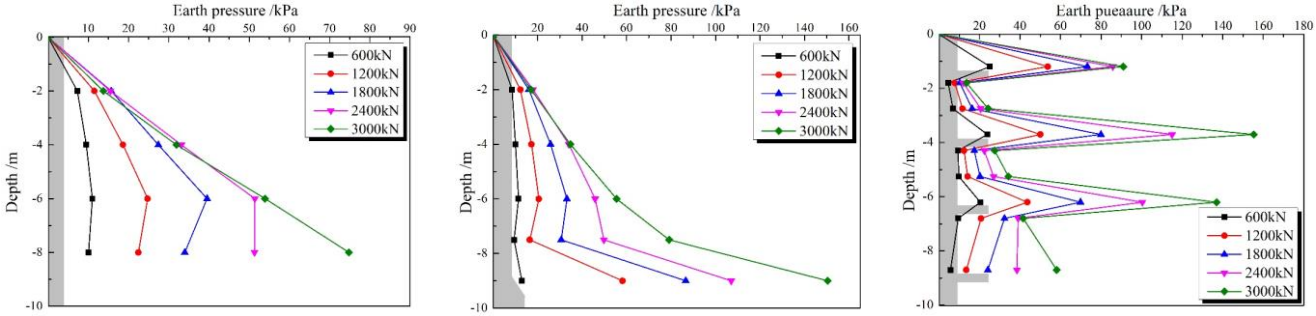

(a) Straight pile (b) Belled pile (c) Roots pile

Fig. 9 Distribution curves of vertical earth pressure

maximum value of the skin friction resistance is at the position of -6 m of the pile body, but with increasing load, the skin friction resistance at the belled base increases significantly. When the applied load reaches a value of 3000 kN, the skin friction resistance at the belled base is approximately 137% of the maximum skin friction resistance of the pile body. However, even when the load of the root pile is small, the skin friction resistance at the root position plays an obvious role. When the apllied load equal to 600 kN, the skin friction resistances at the roots of each layer are 30.8 kPa, 28.3 kPa, 23.4 kPa and 10.6 kPa, respectively. The skin friction resistance at the first layer is the most obvious. With increasing the loads, the skin friction resistance of the deep layer gradually plays a major role. When the load is 3000 kN, the root skin friction resistances of each layer are 111.5 kPa, 184 kPa, 157 kPa and 109 kPa. The position of the maximum skin friction resistance of the roots is transferred from the first layer to the second layer. This shows that the exertion of root uplift resistance has a depth effect to a certain extent, that is, the uplift resistance of roots in the upper layer is exerted earlier than that in the lower layer. Therefore, the design principle of the multilayer layout is the premise to ensure the stable exertion of root uplift resistance in the whole loading process.

3.4 Development law of the earth pressure around a pile

Fig. 9 shows the distribution curves of vertical earth pressure under different loads. With increasing the applied load, the earth pressure increases, but the increase range is obviously different at different depths. When the load is small, the earth pressure around the straight pile first increases and then decreases with depth. With increasing the applied load, the increase in deep earth pressure gradually becomes obvious. Under the ultimate load, the earth pressure near the pile bottom increases most significantly. The variation in earth pressure around the upper pile body of the belled pile with depth is similar to that of the straight pile. While, the increase in soil pressure near the belled base is not obvious under a small load, but the earth pressure around the belled base is obvious with increasing load. However, the influence of the belled base on the upper part of the soil does not change significantly with increasing load, and the earth pressure value of the measuring point at the level of 7.5 m is always similar to that elsewhere along the pile body. Therefore, the influence range of the belled base should not be greater than $1.5h_b$.

The earth pressure of the root pile has an obvious mutation around the roots: the earth pressure above the roots increases significantly, while the earth pressure below the roots decreases slightly compared with the upper part of the pile body. This shows that with increasing the loads, the top surface of the roots contributes to the uplift resistance. However, due to the relative displacement between the pile and soil, a separation of contact surfaces between the bottom surface of the roots and the soil has been appeared, which cause reduction in the uplift resistance of the soil in a small range near the bottom of roots. However, by making a comparison with the setting of the belled base at the bottom of the pile, the setting of multilayer roots can make the soil in a wider range bear the load synchronously and fully utilize skin friction resistance and end resistance of the soil at different depths.

Table 2 Numerical calculation conditions for the simulated root pile tests (#3~16)

Number	Length of roots /(m)	Location of roots /(m)	Number of roots in each layer
3	0.3	-1.6/-2.2/-2.8/-3.4	6
4	0.3	-1.6/-2.8/-4/-5.2	6
5	0.3	-1.6/-4.1/-6.6/-9.1	6
6	0.6	-1.6/-2.2/-2.8/-3.4	6
7	0.6	-1.6/-2.8/-4/-5.2	6
8	0.6	-1.6/-4.1/-6.6/-9.1	6
9	1.2	-1.6/-2.2/-2.8/-3.4	6
10	1.2	-1.6/-2.8/-4/-5.2	6
11	1.2	-1.6/-4.1/-6.6/-9.1	6
12	0.6	-1.6/-4.1/-6.6/-9.1	4
13	0.6	-1.6/-4.1/-6.6/-9.1	8
14	0.6	-1.6/-4.1/-6.6/-9.1	10
15	0.6	-1.6/-4.1/-6.6/-9.1	14
16	0.6	-1.6/-4.1/-6.6/-9.1	/

4. Bearing characteristics of piles under multilayer root interactions

4.1 Model establishment and parameter selection

To further explore the influence of multilayer root interactions on the bearing performance of piles, 16 groups of numerical calculation models have been done with taking into consideration the following parameters: different root spacing, root lengths and root densities (number of roots) in one layer (Table 2). The previous mentioned calculation have been accomplished by using ABAQUS software. Among them, numerical simulations #1 and #2 correspond to the uplift test of the on-site straight pile and belled pile, respectively. Numerical simulations #3-16 correspond to the uplift test of the root pile under the conditions of different root lengths, spacing and root densities (number of roots) in one layer, of which numerical simulation #8 corresponds to the field pull-out test of the root pile. The length of the root pile is 10 m, and the diameter is 1.2 m. Four layers of roots are arranged in total. The height of the roots is 0.3 m, the thickness is 0.15 m, and the lengths are considered as 0.3 m, 0.6 m and 1.2 m in different working conditions, respectively. The details are shown in Fig. 10. The roots in one layer are designed with 4, 6, 8, 10 and 14 pieces/layer and discs in different working conditions. The specific calculation conditions of the root pile are shown in Table 2. The soil in the model is a cylinder with a diameter of 40 m and a height of 20 m. The radial size of the soil is much larger than the pile diameter, which can effectively eliminate boundary effects. The basic information of the model is shown in Fig. 11.

The loading is carried out by displacement control. According to the relevant specifications, the pile failure standard can be set according to the following conditions: (1) the displacement reaches 100 mm; (2) the displacement of the pile top under a certain level of load is more than 5 times that of the previous level of load. According to the loading mode adopted in this paper, the ultimate load of the pile can be judged according to whether there is an obvious increment of load on the top of the pile under increasing displacement.

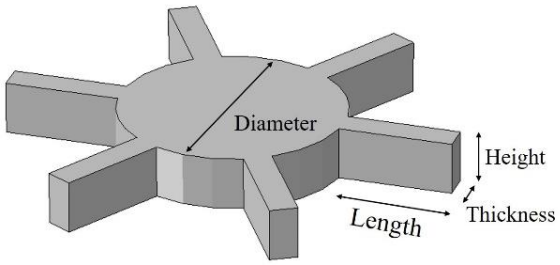

Fig. 10 Roots design parameters

The pile and soil model adopts a hexahedral mesh. In the analysis of pile-soil interaction, the soil is usually considered as a semi-infinite body. Therefore, when the model scope is sufficiently large, it can be assumed that the model boundaries are not influenced by foundations. Based on the current research result (Liu *et al*. 2023, Xu *et al*. 2020), the bottom constraint of the soil model is U1 = U2 = U3 = 0, and the side constraint of soil is U1 = U2 = 0. In the production of piles, the bell and the roots are considered to be integrated with the pile body, so they are both connected by “tie” constraints with the pile body in numerical simulation.

On the aspect of material constitutive model selection, the tested pile is a linear elastic model, and the soil model is a Mohr–Coulomb elastic–plastic model. Due to the large difference in the properties between miscellaneous fill and undisturbed soil and the small difference in the parameters between silt and silty clay in undisturbed soil, the soil in the model is divided into two layers, of which 0~2 m is miscellaneous fill (soil 1) and 2~22 m is undisturbed soil (soil 2). In pile-soil contact, the tangential contact is a "penalty" contact, the normal contact is a "hard" contact, and the friction coefficient is 0.6. Existing studies have shown that (O'Neill 2001, Kulhawy 1979) the lateral pressure coefficient has an obvious impact on the

Table 3 Mechanical parameters of the numerical model

Material	Density γ/kg·m^{-3}	Elastic modulus E/MPa	Poisson's ratio μ	Cohesion c/kPa	Internal friction angle φ/°
Pile	2.45	3e4	0.15	/	/
Soil 1	1.4	6	0.3	23	20
Soil 2	1.6	15	0.3	23	20

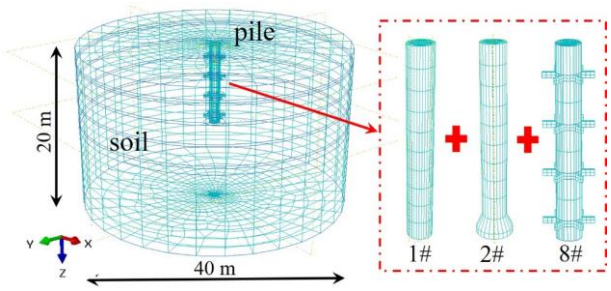

Fig. 11 Basic information of the numerical model

foundation uplift resistance, and the square root $\sqrt{K_p}$ of the passive earth pressure coefficient in the process of foundation uplift is more in line with the development law of foundation uplift resistance. Therefore, the lateral pressure coefficient in this paper is 1.43, and the physical and mechanical parameters of the pile-soil in the model are shown in Table 3.

4.2 Model validation

Fig. 12 is the comparison of the *Q*-*S* curves between the field test and numerical simulation. Within the test load range, the field test load–displacement curves of different piles are basically consistent with the load–displacement curves of the numerical simulation. Only the displacement of straight piles under the limit load (2700 kN in the field test and 2657 kN in the numerical simulation) exhibits a certain divergence. In summary, the numerical simulation parameters and methods selected in this paper can better reflect the actual deformation of piles on site.

4.3 Influence of root spacing and length on the bearing characteristics of multilayer root piles

4.3.1 Variation law of uplift resistance

Fig. 13 shows the *Q*-*S* curves of piles with different root lengths and spacing. Under the condition of the same longitudinal root spacing, the pile uplift resistance increases with increasing root length, and the maximum linear displacement also increases with increasing root length. Under the condition of the same root length, the larger the root spacing is, the higher the uplift resistance; additionally, with a slower the development of the displacement curve, the maximum linear displacement increases significantly, and the curve transitions from a "sudden change" form to a "gradual change" form. This shows that the increase in the

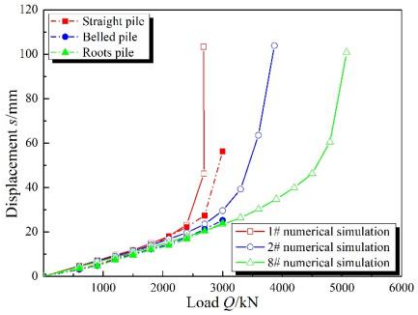

Fig. 12 Comparison of the *Q*-*S* curve between the field test and numerical simulation

length and spacing of the roots can effectively reduce the relative slip between the pile and soil and that increasing in the depth of the root setting position can effectively inhibit the large displacement caused by the premature plastic failure of the soil.

Furthermore, the variation in the ultimate uplift resistance of the pile with different root spacing and lengths is shown in Fig. 14. The ultimate uplift resistance of the foundation increases slowly and then rapidly with increasing root spacing, while the ultimate uplift resistance increases rapidly and then slowly with increasing root length, and the above trends are more obvious with increasing root spacing and length. The ultimate uplift resistance of the pile with a 0.6 m (1R) root spacing is approximately 57%~75% of that with a 2.5 m (approximately 4R) root spacing, while the ultimate uplift resistance of the pile with a 1.2 m (2R) root spacing is approximately 66%~80% of the 2.5 m root spacing. The spacing of the roots has a greater impact on the uplift resistance than the length of the roots. Therefore, the design principle of root piles should primarily ensure sufficient longitudinal root spacing, and the root length is the secondary factor.

4.3.2 Distribution characteristics of skin friction resistance

Fig. 15 shows the skin friction resistance distribution curves with different root lengths and spacing. The skin friction resistance under different loads increases with increasing depth. Among them, the skin friction resistance at the position of the roots changes most obviously with depth. The skin friction resistance at the root layer increases approximately linearly with depth (there is a certain nonlinear change in skin friction resistance between the first layer and other layers of roots), which is mainly due to the low strength of the soil where the first layer of roots is located. However, there are some differences in the variation law of the skin friction resistance under different root spacing and lengths.

The uplift resistance of roots increases with increasing the root spacing as a whole. When the distance between the roots is 0.6 m, the skin friction resistances of the roots and pile body, which is between the two layers, will significantly be improved. The difference between the two is small. This is mainly because the normal load of the roots causes the soil to undergo extrusion deformation in a small

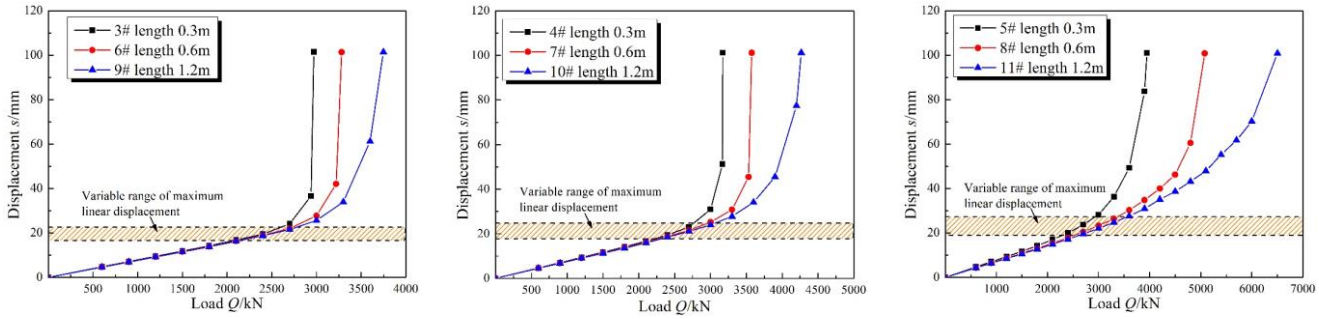

(a) 0.6 m (b) 1.2 m (c) 2.4 m

Fig. 13 *Q*-*S* curves of piles with different root lengths and spacing

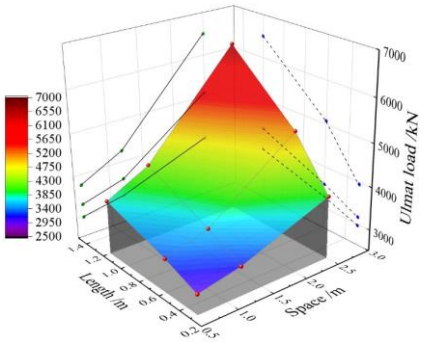

Fig. 14 Variation in the ultimate uplift resistance of the pile with different root spacing and lengths

range, which increases the lateral stress and improves the skin friction resistance of the soil between the two layers of roots. When the distance between the roots is 1.2 m, the skin friction resistance of the roots is significantly higher than that between the two layers of roots, but at this time, the skin friction resistance between the two layers of roots is still higher than that at other positions outside the root setting area. Under the condition of this spacing, there is still a certain interaction between two adjacent layers of roots. When the spacing between the two layers of roots is 2.5 m, the skin friction resistances of the roots and the pile body basically do not affect each other. The skin friction resistance of the pile body between the two layers of roots is positively correlated with the depth. The skin friction resistances of the adjacent depths above and below the roots are similar. At this time, the root spacing is the critical distance to consider to eliminate the interaction between adjacent layers of roots.

Under the influence of different root lengths, the root skin friction resistance increases with increasing root length, but the increasing amplitude decreases gradually. Taking the fourth layer of roots in Fig. 15(b) as an example, when the length of the roots is doubled, the ultimate uplift resistance increases by approximately 35%, while when the length of the roots is tripled, the uplift resistance increases by only 88%. In addition, when the spacing between the two layers of roots is small, the pile body skin friction resistance between the two layers of roots also increases with increasing root length.

In summary, a small spacing will increase the shear strength of the soil between two layers of roots to a certain extent; the longer the key roots are, the more obvious the effect is. However, the interaction of the roots under a small spacing will also lead to a significant reduction in uplift resistance (the reduction degree is much greater than the increase in the skin friction resistance of the pile body). The effect of the length on the lifting of the uplift resistance of the roots is not linear. When the roots are too long, the lifting effect of the uplift resistance is limited, and there is a risk of bending failure.

To further quantitatively analyse the influence of different root spacing and length conditions on the exertion of uplift resistance, the reduction coefficient of the uplift resistance of the interlayer roots ψ, which is the ratio of the uplift resistance of the roots to the uplift resistance of roots with different root lengths at the critical spacing (when the root spacing exceeds the critical spacing, ψ=1), is considered. The spacing ratio h_s/h_{smax} is the ratio of the root spacing to the critical spacing, which eliminates the interaction between the adjacent layers of roots, and the diameter length ratio r/l. Taking the ultimate load as an example, the coefficients ψ calculated by different spacing ratios h_s/h_{smax} and diameter length ratios r/l are shown in Fig. 16. It is found that the relationship between ψ, h_s/h_{smax} and r/l conforms to the development law of the exponential function in Eq. (4). When the spacing is small (< 0.5), the reduction coefficient ψ increases rapidly with increasing spacing ratio h_s/h_{smax}, up to 0.7~0.9, but the root diameter length ratio r/l has less of an impact. When the spacing is large (> 0.5), the reduction coefficient ψ increases slowly with increasing spacing ratio h_s/h_{smax}, only 0.1~0.3, but the root diameter length ratio r/l has an obvious impact.

$$\psi = aEXP\left[\frac{-\left(\frac{h_s}{h_{s\max}}\right)^{\left(\frac{r}{l}\right)^{0.25}}}{t}\right] + b \tag{4}$$

Where a, b and t are fitting parameters, a=-1.049, b=1.051, t=0.341; h_{smax} is the the maximum spacing when there has the influence between two layers of roots; r is the radius of the pile; and l is the length of the pile.

4.3.3 Distribution law of the influence range of interlayer roots

Fig. 17 shows the stress increment contour map at the

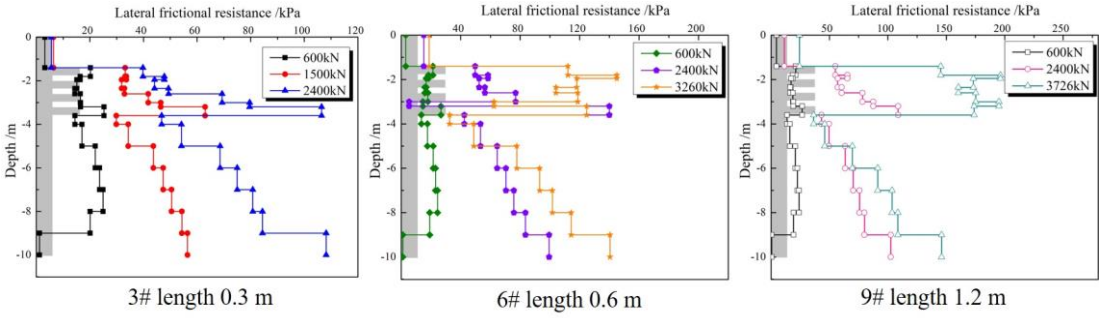

(a) The spacing is 0.6 m

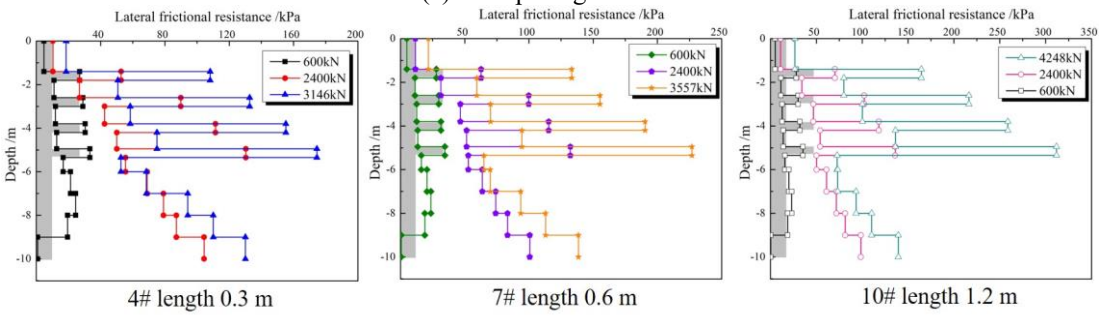

(b) The spacing is 1.2 m

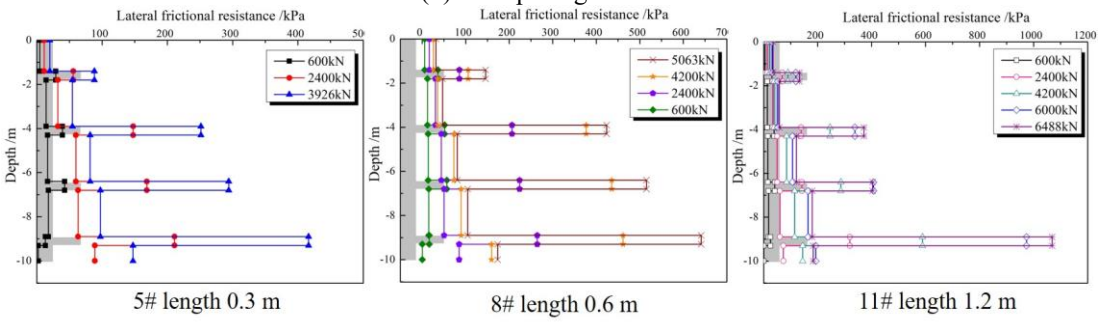

(c) The spacing is 2.4 m

Fig. 15 Skin friction resistance distribution curves (#3~11)

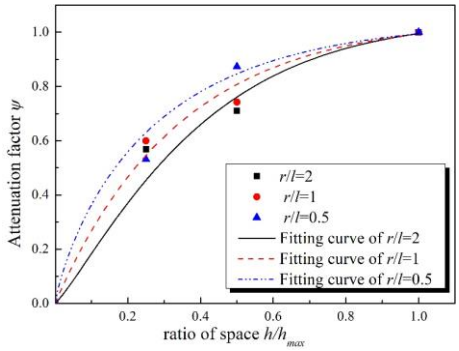

Fig. 16 Root uplift resistance under the influence of length and spacing

ultimate load. In general, the increment of stress near the roots increases with increasing depth. The influence range and distribution form of roots are obviously affected by the change in root spacing and length. When the spacing is small (0.6 m), the influence range between two adjacent layers of roots is basically a "rectangular" distribution and changes little with depth. At this time, the influence of the stress field between similar roots is obvious. With increasing the roots spacing (1.2 m), the distribution of the influence range between two layers of roots gradually changes from " rectangular " to "trapezoidal", the horizontal range of influence of roots decreases with the decrease in depth, and the longitudinal influence range of each layer of roots is still completely connected, indicating that there is still a certain influence on the stress field between adjacent layers of roots at this spacing. Through considering further increasing in the spacing (2.5 m), the distribution form of the stress field between roots changes to "beaded", and the influence area of roots in each layer is relatively independent. At this time, the uplift resistance of roots is fully exerted, and the larger spacing eliminates the superposition effect of the stress field between adjacent layers of roots. In addition, through comprehensive comparison, it is found that the longitudinal influence range of the root stress field at different locations is mainly affected by the buried depth of the roots and the root spacing. While, the length of the roots has little effect on the change of the longitudinal influence range. When the spacing between adjacent layers of roots is 2.5 m, the influence range at -1.6 m of the first layer of the roots can

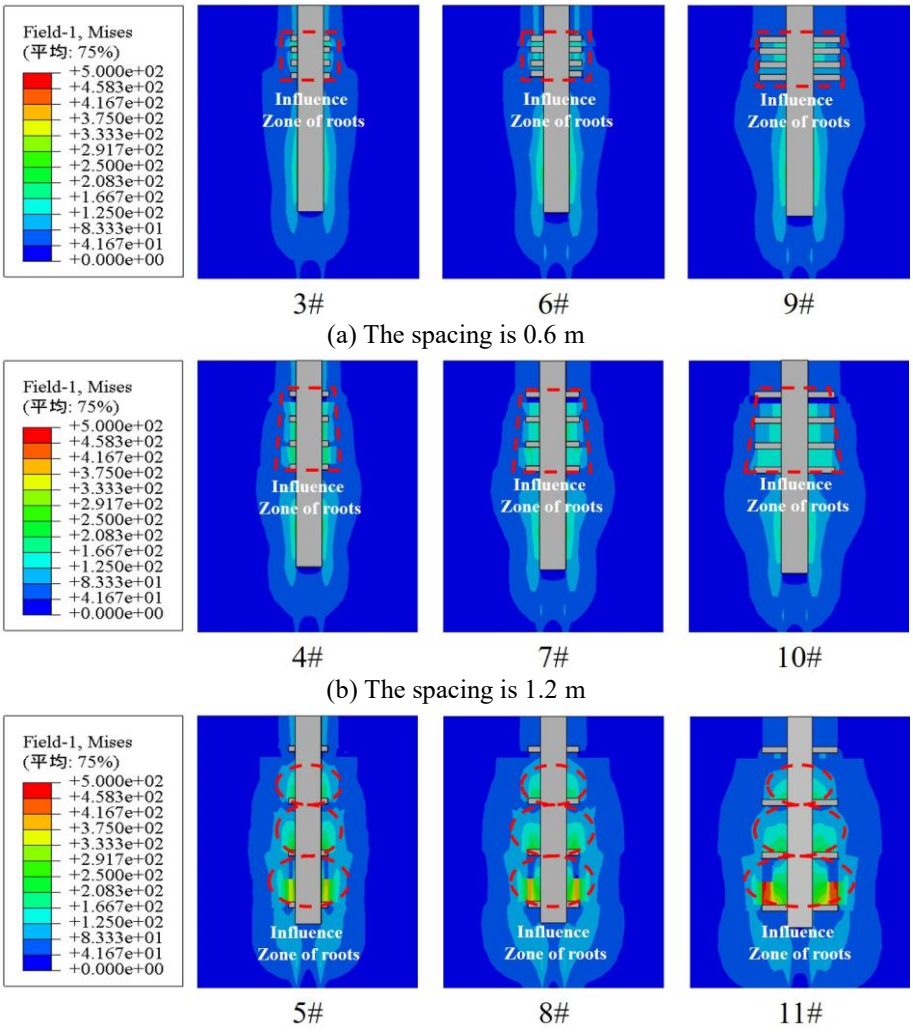

(a) The spacing is 0.6 m

(b) The spacing is 1.2 m

(c) The spacing is 2.4 m

Fig. 17 Stress increment contour maps

be approximately considered to be connected with the ground surface, the influence range of roots at -4.1 m is approximately 1.8 m, the influence range of roots at -6.6 m is approximately 2 m, and the influence range of roots at -9.1 m is approximately 2.2 m. The longitudinal influence range of roots increases linearly with depth, with an average increase of approximately 0.08 per linear meter.

4.3.4 Pile failure mode

Fig. 18 shows the displacement increment contour maps at the stage of applying the ultimate load. The displacement of the soil around the pile is mainly concentrated at the position of the roots, and the development mode of the displacement field of the soil around the pile is obviously affected by the distance between adjacent layers of roots. When the spacing is 0.6 m (h_s/h_{smax}=0.25), the interaction in the root setting area is strong, and the displacement of roots in the lower layer under the load has an obvious impact on the displacement field of the roots in the upper layer. At this time, the failure mode of the soil around the pile is mainly annular shear failure in the root influence area. When the spacing is 1.2 m (h_s/h_{smax}=0.5), there is an obvious influence between adjacent layers of roots, but when the distance between two layers is far in the root setting area, the interaction degree of roots is small. At this time, the displacement field of the lower layer of roots has a significant influence on its adjacent layer in only the upper part. The failure mode of the soil around the pile is independent shear failure of roots under the influence of the adjacent layer of roots. When the spacing is 2.5 m (h_s/h_{smax}=1), the displacement field between adjacent layers of roots is relatively independent. At this stage, the roots play an independent bearing role, and the failure mode of the soil around the pile is the independent shear failure of the roots. The development mode of the displacement field of the soil around the pile is not significantly affected by the length of the roots, and the length of the roots is positively correlated with only the influence range of the displacement field. When the length of the roots is 0.3 m (0.5r), 0.6 m (1r) and 1.2 m (2r), the maximum influence range of the displacement field is 2.6r, 3.5r and 4.3r respectively.

4.4 The influence of the density of roots in each layer on the uplift resistance

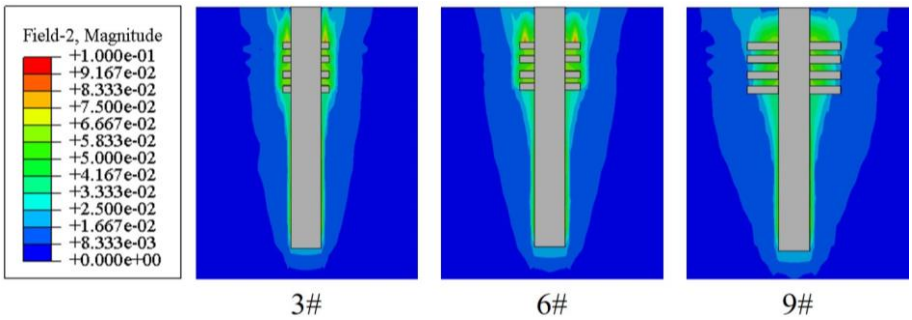

(a) The spacing is 0.6 m

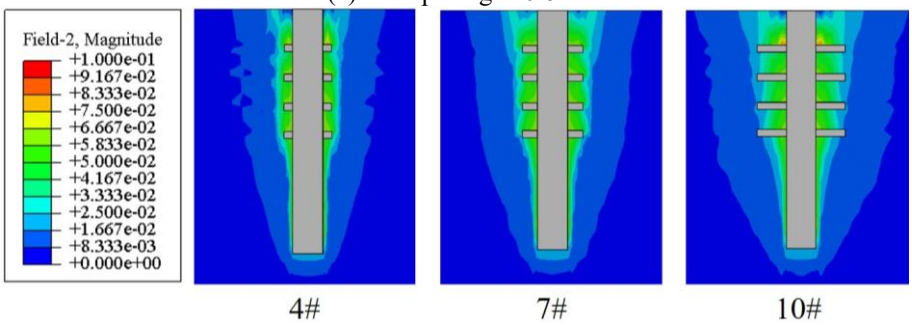

(b) The spacing is 1.2 m

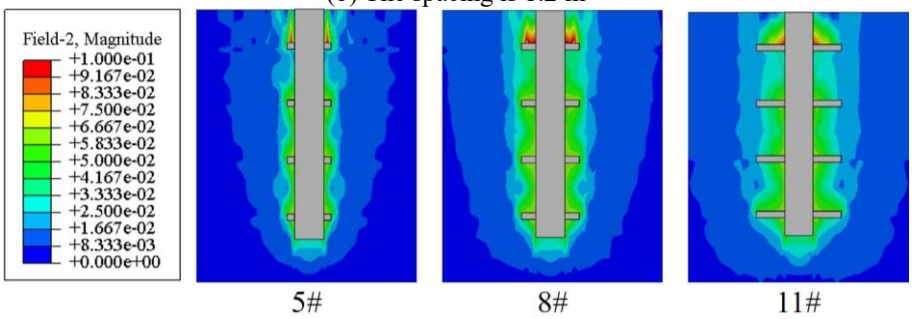

(c) The spacing is 2.4 m

Fig. 18 Displacement increment contour maps

4.4.1 Variation law of uplift resistance

Fig. 19 is the *Q*-*S* curve of piles under different numbers of roots in each layer. Overall, the maximum linear displacement increases with the increase of the root density (number of roots) in each layer, from 15 mm to 30 mm. In general, the ultimate uplift resistance of the pile first increases, then decreases and finally increases with the increase in the root density (number of roots) in each layer. When the number of roots in each layer is less than 8, the ultimate load increases with the increase in root density in each layer. When the number of roots in each layer is 8~14, the ultimate uplift resistance of the pile decreases to a certain extent with the increase in the number of roots. When the number of roots in each layer is 8~14, the ultimate uplift resistance of the pile decreases to a certain extent, but the greater the density of roots in each layer is, the smaller the attenuation degree. When the roots in each layer become a disc, the uplift resistance of the foundation reaches the maximum, but this disc shape cannot be realized in the construction of the pile, so this condition is only an ideal working condition. Thus, a greater root density in each layer cannot consider absolutely better. Much higher of the density makes the roots have a stronger interaction in its

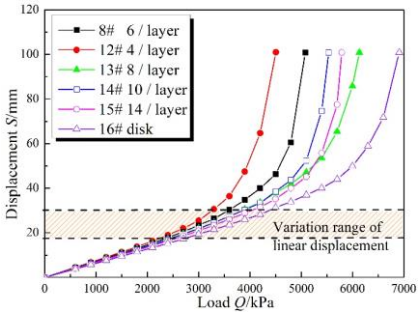

Fig. 19 *Q*-*S* curve of piles under different numbers of roots in each layer

layer, which weakens the uplift resistance of the soil. Under this condition, the number of roots in each layer should be within 8/layer.

4.4.2 Distribution characteristics of skin friction resistance

Fig. 20 shows the skin friction resistance distribution curves at the ultimate load for different densities in each layer. Since the law of skin friction resistance is similar to that discussed in the previous section, only the distribution

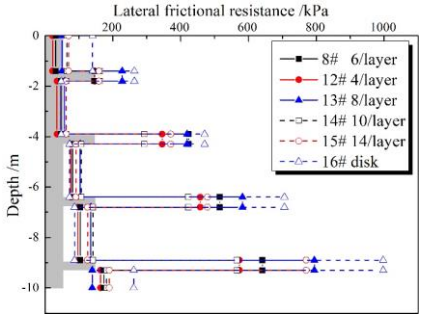

Fig. 20 Skin friction resistance distribution curves at the ultimate load (#8, #12~16)

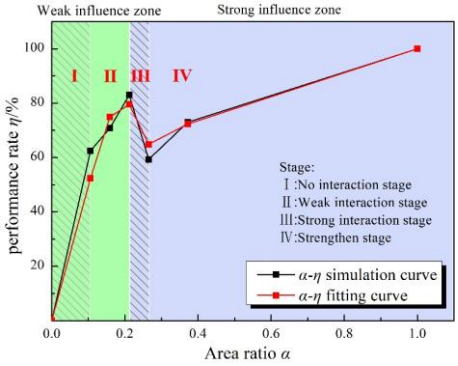

Fig. 21 The uplift resistance performance of roots under the influence of the area ratio

curves at the ultimate load are further investigated. With different root densities in each layer, the uplift resistance at the root position shows an obvious depth effect, and the increase in the uplift resistance is approximately linear with increasing depth. At the same time, the development law of the uplift resistance at the root position with uplift load is basically the same as that of the uplift resistance of the pile. With the increase of the root density in each layer, the trend of skin friction resistance distribution is shown: increasing – decreasing – increasing. The variation range increases with increasing depth.

Taking #16 as a benchmark, root density is converted into the cross-sectional area ratio using Eq. (5) to further investigate the impact of root density (number of roots) on uplift resistance. The exertion degree of uplift resistance in different root densities η is calculated by Eq. (6). The comparison results are plotted in Fig. 19.

$$\alpha = \frac{nBl}{\left(R^2 - r^2\right)\pi} \tag{5}$$

$$\eta = \frac{\sum_{m=1}^{i} Q_{Ri}}{\sum_{m=1}^{i} Q_{pi}} \times 100\% \tag{6}$$

where n is the number of roots, B is the width of roots, l is the length of roots, R is the diameter of the disc, r is the radius of the pile, m is the number of layer, Q_{Ri} is the uplift resistance of the ith layer of roots, and Q_{pi} is the uplift resistance of the disc.

The influence of the cross-sectional area ratio of roots on uplift resistance can be split into weak influence and strong influence zone, as can be shown in Fig. 21. There have two stages at weak influence zone. Stage I is the "no interaction stage," in which there is essentially no interaction between roots in the same layer. As the cross-sectional area ratio α grows, so does the exertion degree of root uplift resistance rapidly. Stage II is the "weak interaction stage", in which has a certain influence between the roots in the same layer, but the degree of influence is small. The exertion degree of the uplift resistance of the roots increases slowly with the increase in the cross-sectional area ratio α. And there also has two stages in strong influence zone. Stage III is "strong interaction stage" which has a strong interaction between roots in the same layer, and the number of roots is not enough to compensate the attenuation of the soil bearing capacity. Stage IV is "strengthen stage" which has a large number of roots at this stage. Although the dense arrangement of roots causes interference between roots in the same layer and seriously weakens the soil bearing capacity. However, the roots and soil between the roots can be viewed as a whole that can make up the loss of uplift resistance due to the interaction when the distance is too small. It shows a slowly increase trend with the increase of area ratio (number of roots). In this paper, the range of different stages is as the following: α<0.1 is stage I, 0.1<α<0.21 is stage II, 0.21<α<0.26 is stage III and 0.26<α<1 is stage IV. In construction, the area sectional ratio should be controlled at stage II which have a high uplift resistance and undergo little interaction.

The model and the range of the values for different stages are given in Fig. 22. The theoretical calculation method is shown in Eq. (7)-(9). β_1 is roots interaction factor and β_2 is the equivalent area ratio factor. Those two factors are chosen to reflect the impact of roots area ratio to uplift resistance performance. The comparison results between theoretical value and numerical value is drawn in Fig. 21. It can be seen that the development law of theoretical calculation results and the numerical calculation results show good agreement. Therefore, the theoretical method can accurately reflect the rule of uplift resistance under different root densities.

$$\eta = \beta_2 \kappa a_R \alpha \ln\left(\beta_1 + 1\right) \tag{7}$$

$$\beta_1 = \frac{\frac{\left(2r + l\right)\pi}{n} - b}{h_R \tan\left(45° + \frac{\varphi}{2}\right)} \tag{8}$$

$$\beta_2 = \begin{cases} 1 & \beta_1 > \dfrac{h_R \tan\left(45° + \varphi/2\right) - b}{{}_R \tan\left(45° + \varphi/2\right)} \\ \left(1 - \dfrac{\left(2r + l\right)\pi - nb}{n\left(h_R \tan\left(45° + \varphi/2\right) - b\right)}\right) & \beta_1 \le \dfrac{h_R \tan\left(45° + \varphi/2\right) - b}{{}_R \tan\left(45° + \varphi/2\right)} \\ \dfrac{\left(2r + l\right)\pi - nb}{nb} + 1 & \end{cases} \tag{9}$$

Where, a_R is fitting parameter, in this paper a_R=0.45. K is the correction coefficient. In stage I and II, K=1. While,

in stage III, K=0.8. when In stage IV, K=0.55. β_1 is roots interaction factor. When β_1>2, the root interaction is at stage I, there is no interaction between roots, take β_1 as 2. When the distance of roots is too close, which means β_1<0.5, it can be consider that the impact of the roots interaction reaches the maximum, when β_1 as 0.5. Because it is assumed that when the interaction effect reaches the maximum, the bearing effect of two roots is the same as that of one. β_2 is the equivalent area ratio factor. When the distance of two pieces is at stage IV, the roots and soil can be regard as a whole. The soil area between roots can be replaced to roots area in a certain. h_R is the height of root. b is the width of root.

4.4.3 Distribution law of the influence range in each layer of roots

In order to better understand the law of different root densities on the influence range of soil, the stress increment of the soil around the pile at the ultimate load is analysed. Only the stress increment contour of the soil at the second layer of roots is chosen as an example since the stress development rules of the soil surrounding the different layer of roots are similar. The stress increment contour map is shown in Fig. 23. When the root density is low, the influence range of the end resistance of the roots on the soil basically extends vertically along the root boundary, the high-stress area is mainly concentrated at the top of roots, whereas the stress between the roots is low. With increasing

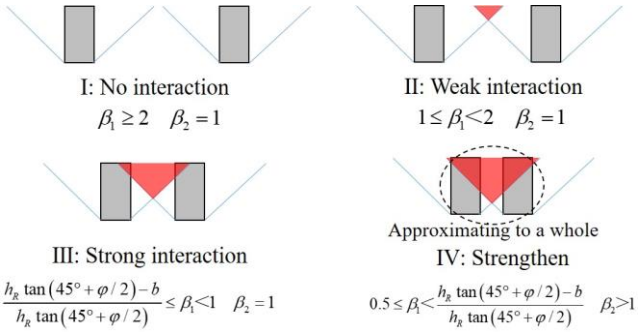

Fig. 22 Model of roots interaction stage

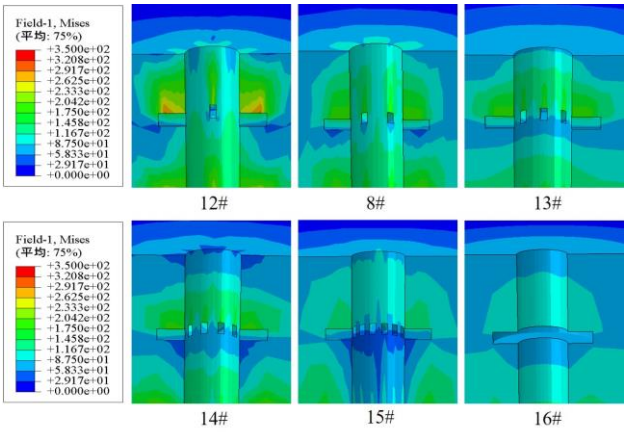

Fig. 23 Stress increment contour distribution of the soil around a pile under different root densities in the 2nd layer

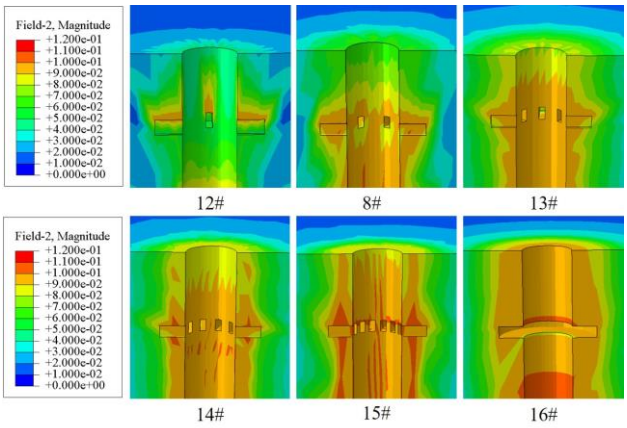

Fig. 24 Displacement increment contour distribution of the soil around piles with different root densities in the 2nd layer

the root density, the peak value of soil stress at the top of the roots decreases accordingly. The high-stress area gradually changes from a strip to a ring distribution on the top of the roots layer, and the stress of the soil was more uniform. However, the soil stress in a small range of approximately 0.5l below the roots decreases gradually with increasing root density. Therefore, the increase of root density in each layer can make the stress distribution on the top of roots layer more uniform effectively. It can prevent the soil reach to plastic failure stage prematurely. But an overly dense arrangement will also reduce the exertion of the bearing capacity of the soil near the bottom of roots within the range of 0.5l.

4.4.4 Pile failure mode

Fig. 24 shows the displacement increment contour distribution of the soil around piles with different root densities in the 2nd layer. When the root density is small (α<0.1), the soil at the top of the roots mainly produces shear failure along the roots, and the shear zone is distributed in strips along the setting position of the roots. With the increasing the root density in each layer, the soil failure mode at the root position gradually evolves from multiple strip shear areas to ring shear areas, and the longitudinal influence range of the ring shear area also increases significantly with the increase in the root density in each layer. Therefore, the increase in root density can effectively prevent the penetration failure of roots, improve the overall deformation resistance of soil, and evolve the overall bearing capacity of a wider range of soil.

5. Nonlinear deformation prediction method of root piles considering multilayer root interactions

5.1 Calculation flow of the uplift deformation of root piles

The analysis in this section has the following assumptions:

(1) The soil mass is homogeneous;

(2) When the root and soil are not damaged, the load distribution of root at different depths is related to the overburden pressure. While When the soil reaches the failure strength, the load of the root at this stage is corresponding to the strength of the soil and does not change anymore with the change of the uplift load; When the root reaches the material strength, the root load at this position will also not change anymore;

(3) The change of the skin friction resistance caused by the root squeezing the soil during the uplift process is ignored.

According to the load transfer method, first, the pile body is divided into n+1 parts based on the position of the root layer, and each part is divided into straight section and roots layer section. Under the action of vertical load Q, the skin friction resistance of the pile body is τ, and the total uplift resistance of the roots is Q_R. The specific load transfer model and calculation process of the root pile are shown in Fig. 25, and the specific calculation method is as the following:

(1) Initial load: Assuming that the uplift load is Q and the total uplift resistance of the root under this load is Q_R, the uplift resistance of the pile body is Qt=Q-Q_R, where Q_R=Q_{R1}+Q_{R1}+…+Q_{R}n. Because the exertion of the root uplift resistance has a depth effect and the exertion of the uplift resistance develops approximately linearly with increasing depth, its load distribution relationship can be calculated by Eq. (10).

$$Q_{Ri}=\frac{\overline{\gamma}_i h_i}{\sum_{j=1}^{n}\overline{\gamma}_j h_j}Q_R \tag{10}$$

where h_i is the burial depth of the ith layer of roots, $i\leqslant n$. $\overline{\gamma}_i$ is the average weight of soil at the ith layer of roots.

(2) Displacement of pile: The root displacement of ω_{Ri} is calculated by $Q_{Ri,}$ the displacement relationship between the top of the roots and the bottom of the pile body in the ith part

$$\omega_{Ri}=\omega_{ti} \tag{11}$$

Therefore, the skin friction resistance can be calculated by the displacement of the pile bottom in the ith part, and then the deformation of the pile body in the ith part can be obtained $\delta\omega_{ti}$. The top displacement of the ith part is ω_i=ω_{ti}+$\delta\omega_{ti}$. Finally, the displacement of the top of the test pile is ω=ω_{t1}+ω_{t2}+…+ω_{tn}.

(3) Continuity detection: If the absolute value of the difference between the calculated value and the assumed value is a very small value δ, it can be considered that the displacement under this condition is the real displacement under load Q. If the result is greater than δ, it is considered that the assumed root and pile loads under this condition do not meet the requirements, and it is necessary to reassume the root load for calculation until the continuity requirements are met.

$$\left|\left(\sum_{i=1}^{n}Q_{Ri}+\sum_{i=1}^{n+1}Q_{ti}\right)-Q\right|\leq\delta \tag{12}$$

(4) Ultimate uplift resistance judgement: The calculated exertion degrees of the uplift resistance of the roots and pile body are judged. When $Q_R\geq Q_{Rult}$, take Q_R=Q_{Rult}; when $Q_t\geq Q_{tult}$, take Q_t=Q_{tult}. At this time, the pile displacement is calculated again, and the resulting load is the ultimate load of the test pile.

5.2 Differential equation of uplift deformation of root pile

From the balance equation of force

$$\frac{dQ(z)}{dz}=-u\tau(z) \tag{13}$$

From the stress–strain relationship

$$Q(z)=-A_pE_p\frac{d\omega(z)}{dz} \tag{14}$$

Combining Eqs. (11) and (14) yields

$$\frac{d^2\omega(z)}{dz^2}=\frac{u}{A_pE_p}\tau(z) \tag{15}$$

where $\omega(z)$ is the axial displacement of the pile body at the calculation point; $\tau(z)$ is the skin friction resistance at the calculation point; z is the depth at the calculation point; A_P is the sectional area of the pile body; and E_P is the elastic modulus of the pile.

5.3 Calculation model of skin friction resistance and root resistance

5.3.1 Calculation model of skin friction resistance

The exertion of skin friction resistance is closely related to the relative pile-soil displacement. The hyperbolic function has been found by many scholars to have the best prediction result for the real displacement. In this paper, Castelli's (1992) measured hyperbolic load transfer function is used, and its expression is

$$\tau=\frac{\omega(z)}{\frac{r}{G_s}\ln\left(\frac{r_m}{r_s}\right)+\frac{\omega(z)}{(K\gamma\tan\varphi)+c}} \tag{16}$$

where r is the pile radius; r_s is the horizontal distance from the pile axis to the calculation point; and r_m is the influence radius of soil shear deformation around pile. Based on Randolph's research results (Randolph and Wroth 1978), r_m=$\chi_1\chi_2(1\text{-}\mu)h$ for the straight pile, where χ_1=2.5 and χ_2=1. γ is the soil weight, φ is the internal friction angle, c is the cohesion, and K is the lateral pressure coefficient. Many studies have shown that for the uplift resistance of piles, when the lateral pressure coefficient adopts the square root of the passive earth pressure coefficient $\sqrt{K_P}$, the calculated result is the closest to the measured value. G_s is the shear modulus of the soil around the pile. When the shear modulus has no test parameters, it can be obtained from Eq. (17):

$$G_s=\frac{E_s}{2(1+\mu)} \tag{17}$$

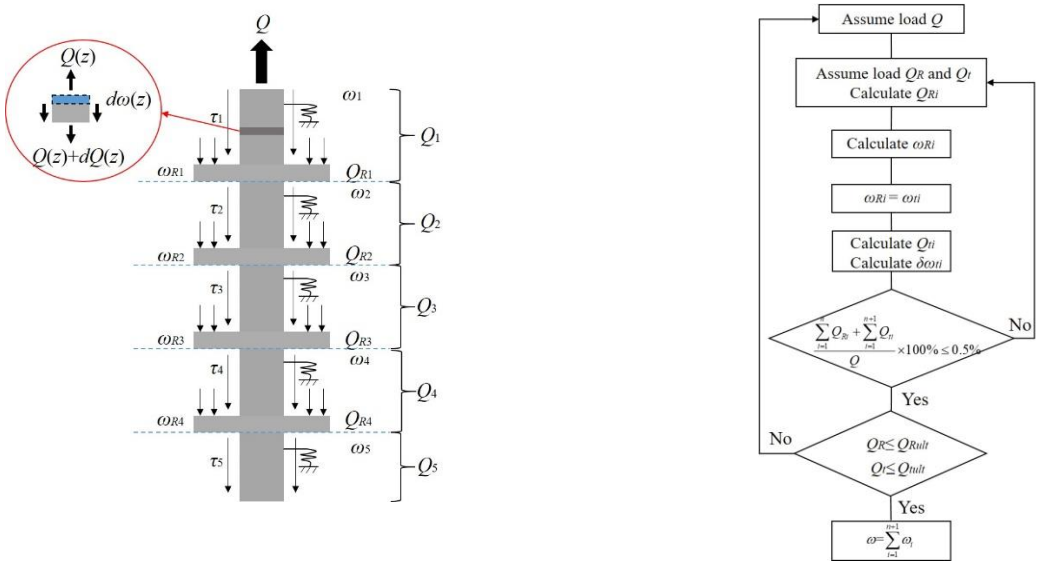

(a) Load transfer model (b) Calculation process

Fig. 25 Load transfer model and calculation process for a root pile

Where: E_s is the compression modulus of the soil, which is generally 2~5 times the elastic modulus. In this paper, E_s=2.5E.

In addition, based on the research results in the previous section, when the pile displacement is within 0~20 mm, the pile-soil displacement is mostly in the elastic deformation stage. At this time, the relative displacement of the pile-soil is small, so it can be approximately considered that the displacement of the pile is the same as the displacement of the soil. When the pile displacement is greater than 20 mm, the displacement gradually shows a nonlinear behaviour of elastic–plastic deformation, resulting in obvious relative displacement between the pile and soil (Wang 2013, Yao *et al*. 2012). Therefore, a quantity factor λ reflecting the relative slip between the pile and soil is introduced to correct the resistance under a large deformation. The relative pile-soil slip at the ultimate load is taken as 20% of the total displacement, so Eq. (16) is corrected as

$$\tau=\frac{\lambda\omega(z)}{\frac{r_0}{G_s}\ln\left(\frac{r_m}{r}\right)+\frac{\omega(z)}{\left(\sqrt{K_p}\gamma\tan\varphi\right)+c}} \tag{18}$$

$$\lambda=1-\frac{\omega(z)-\omega_0}{\omega_{\max}-\omega_0}0.2 \tag{19}$$

Where: ω(z) is the displacement at the calculation position; $\omega_{\max}$ is the relative displacement at the ultimate load, 100 mm; and ω_0 is the maximum elastic displacement, 20 mm.

5.3.2 Calculation model of root resistance

Zhang *et al*. (2013) deduced the deformation calculation method of the belled base of the belled pile based on elastic theory and predicted the nonlinear deformation of the belled pile by introducing the quadratic term. The model at the pile bottom is simplified to a rigid ring, as shown in Fig. 26, and the deformation calculation method of the belled base is as follows

$$\omega(z)=\frac{Q_b(1+\mu)}{\pi\left(R^2-r^2\right)E_s}\left(\cos\beta_1-\cos\beta_2\right)\left[1+\frac{2(1-\mu)}{\cos\beta_1\cos\beta_2}\right]z \tag{20}$$

When the calculation position is the bottom of the belled base $z\rightarrow0$, the above expression can be simplified as

$$\omega(z)=\frac{Q_b(1\text{-}\mu)}{\pi(R+r)G_s} \tag{21}$$

At this stage of calculation, the expression is still the relationship between load and displacement under linear conditions. Since the soil in the uplift process cannot be regarded as an elastic semi-infinite body, it is necessary to introduce a quadratic term to modify the relationship between load and displacement, as shown in Eq. (22).

$$\omega(z)=\frac{(1-\mu)}{\pi(R+r)G_s}\left(Q_b+\xi Q_b^2\right) \tag{22}$$

Where: ξ is a parameter considering the strength properties of the soil. The higher the soil strength is, the smaller ξ is. In this paper, 1/800 is taken.

In addition, it is known from the previous section that the root uplift resistance is affected by the influence of root spacing and length. Thus, the actual root uplift resistance Q_R=ψQ_{Rmax}, where Q_{Rmax} is the root uplift resistance under critical spacing and ψ is the reduction coefficient of the uplift resistance of the interlayer roots. The root uplift resistance under different layer densities can be equivalently replaced by studying the relationship between the cross-sectional area ratio α and the uplift resistance exertion degree η, so the root uplift resistance can be corrected as Q_R=$\eta\psi Q_b$. Finally, the expression after replacement is Eq. (23), in which the relationship between η and α is given by Eq. (7)-(9).

$$\omega(z)=\frac{(1-\mu)}{\pi(R+r)G_s}\left[\frac{Q_R}{\psi\eta}+\xi\left(\frac{Q_R}{\psi\eta}\right)^2\right] \tag{23}$$

Table 4 Parameters of soil strength

Material	Depth H/m	Density γ/kg·m^{-3}	Elastic modulus E/MPa	Poisson's ratio μ	Cohesion c/kPa	Internal friction angle φ/°
Soil 1	2	1.4	6	0.3	23	20
Soil 2	10	1.6	15	0.3	23	20

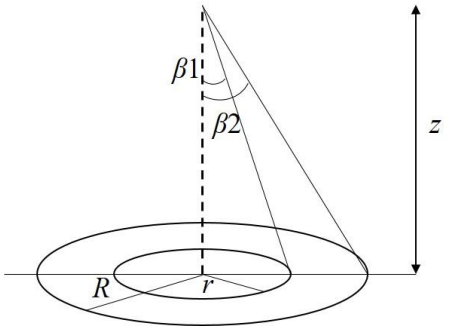

Fig. 26 Stress model of a soil ring under compression

5.4 Calculation model of the ultimate uplift resistance of roots

The uplift resistance of the roots mainly includes the self-weight of the soil on the top of the roots and the shear strength of the soil within the influence range. Assuming that the additional stress of the soil within the influence range caused by the uplift process decays linearly along the longitudinal direction to the influence boundary, the ultimate uplift resistance can be calculated according to the following Eq.

$$Q_R = \sum_{i=1}^{n} \alpha \gamma h_i \left(R^2 - r^2\right)\pi + \eta R \pi h_{hi} \tau_{ult} \tag{24}$$

Where: h_{ei} is the longitudinal influence range of the ith layer of roots. When $h_{eimax} \geq h_{is}$, $h_{ei} = h_{is}$. When $h_{eimax} \leq h_{is}$, $h_{ei} = h_{eimax}$, where h_{eimax} is the maximum longitudinal influence range under the condition that the roots do not interact.

5.5 Example verification

To more accurately reflect the difference between theoretical calculations, field experiments and numerical simulation results under different root parameters, the field experiments of root piles and numerical simulations #3, #8, #10 and #15 are selected to calculate the deformation under various design parameters. The length of the pile is 10 m, and the diameter is 1.2 m. The width of the roots is 0.3 m, the thickness of the roots is 0.15 m, and the lengths of the roots are 0.3 m, 0.6 m and 1.2 m, respectively. Four layers of roots are set along the pile, and the number of roots in each layer under different conditions are 4 pieces/layer, 6 pieces/layer and 14 pieces/layer. The strength parameters of the pile are E=3×10^4 MPa and μ=0.15. The soil is divided into two layers: the depth range of the first layer is 0~-2 m, and the depth range of the second layer of soil is -2~-10 m. The specific parameters of the soil are shown in Table 4.

Fig. 27 shows a comparison of the theoretical, numerical simulation and experimental values. Under the conditions of

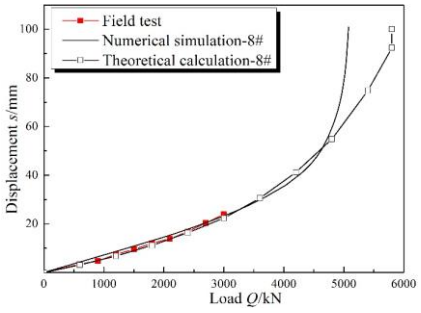

(a) 8#

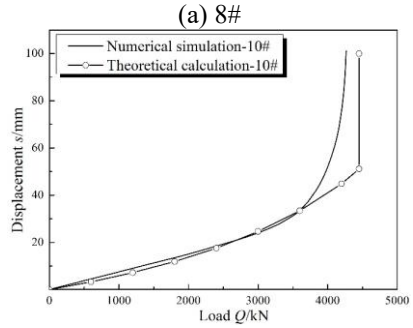

(b) 10#

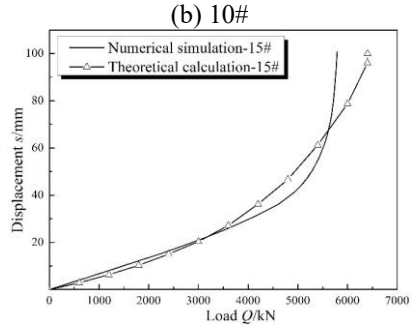

(c) 15#

Fig. 27 Comparison of the theoretical, numerical simulation and experimental values

the load test, the theoretical calculation results have a high degree of coincidence with the field test results. Compared with the numerical simulation, when the displacement is small (<40 mm), the theoretical calculation and the numerical simulation have a high degree of coincidence.

With the increase in displacement, the theoretical calculation curve and the numerical simulation curve have different degrees of divergence, and the theoretical value is larger than the limit load obtained from the numerical simulation, of which those of #8 increases by approximately 11.4%, #10 by approximately 4.3%, and #15 by approximately 10.5%. In general, although there is a certain divergence in the theoretical calculation value under the condition of large displacement, the difference is small, which can accurately reflect the nonlinear deformation development law of the root pile under the action of a large load.

6. Conclusions

• Under the maximum test load, the displacement of the belled pile and root pile is only 45% and 42.6% of that of the straight pile. The appropriate setting of the roots and belled base can effectively control the pile displacement. However, the exertion of belled base resistance lags behind that of the skin friction resistance, and the setting of multiple layers of roots along the pile depth can make the root resistance and skin friction resistance work simultaneously so that the soil at different depths can be stressed together, and the ultimate uplift resistance of pile can be improved to a greater extent.

• Increasing the root length and spacing can effectively reduce the relative slip between the pile and soil and improve the uplift resistance of the pile. However, increasing the root spacing is better than increasing the root length. When h_s/h_{smax}<0.5, the uplift resistance increases rapidly with increasing spacing, but the change in r/l has little effect on the change in ψ. When h_s/h_{smax} > 0.5, the situation is the opposite. In addition, the longitudinal influence range of roots is mainly affected by the embedment depth of roots, while the change in root length has little effect.

• According to the influence area of adjacent roots in the same layer, the uplift resistance influenced by roots density shows 4 stages: stage I no interaction, stage II weak interaction, stage III strong interaction and stage IV strengthen. In construction, the area sectional ratio should be controlled at stage II which have a high uplift resistance and undergo little interaction.

• The root spacing between layers affects the overall failure mode of the pile. When h_s/h_{smax}<0.5, the mode of failure of the pile is circular shear failure at the root setting area. When 0.5≤ h_s/h_{smax}<1, the mode of failure of the pile is independent shear failure affected by root interactions at the root setting area. When h_s/h_{smax}≥1, the mode of failure of the pile is independent shear failure at the root setting area. The density of roots in each layer affects the root failure mode. When the cross-sectional area ratio α< 0.16 (6 pieces/layer), the roots produce banded shear failure on their tops. When the cross-sectional area ratio α>0.16, the roots produce circular shear failure in their respective layer. However, the length of the roots has little effect on the mode of failure of the pile.

• Based on the load transfer method, the roots pile nonlinear deformation calculation method under uplift load is established. This method not only considered the influence of different stress conditions and roots positions on load distribution of roots, but also considered the influence of roots interaction at same layer and between layers on uplift resistance. The prediction of the nonlinear deformation and the development of "sudden change" displacement in the failure stage of roots pile is realized. The results have a high degree of coincidence with the corresponding field test and numerical simulation results and thus can reflect the actual deformation law of root piles.

Acknowledgments

This work was supported by the Qinghai Electric Power Company Limited (52283820000A), the Northwest Electric Power Design Institute Co., Ltd. of China Power Engineering Consulting Group (XB1-TM05-2017) and the National Natural Science Foundation of China (Grant Nos. 41972266 and 41772319). Moreover, the authors gratefully thank the editors' and anonymous reviewers' suggestions and comments.

References

AbdelSalam, S.S., Suleiman. M.T. and Sritharan, S. (2014), "Modeling load-transfer behavior of H-piles using direct shear and penetration test results", *Geotech. Test J.*, **37**(4).

Boonyatee, T. and Lai, Q.V. (2020), "A non-linear load transfer method for determining the settlement of piles under vertical loading", *Int. J. Geotech. Eng.*, **14**(2), 206-217. https://doi.org/10.1080/19386362.2017.1410337.

Cooke, R.W., Price, G. and Tarr, K. (1979), "Jacked piles in London Clay: a study of load transfer and settlement under working conditions", *Geotechnique*, **29**(29), 113-147. https://doi.org/10.1680/geot.1979.29.2.113.

Castelli, F., Maugeri, M. and Motta, E. (1992), "Analisinon lineare delcedimento diun Palo Singolo", *Ital Geotech. J.*, **26**(1), 115-135.

Chalmovsky, J. and Mica, L. (2020), "Prediction of the load-displacement response of ground anchors via the load-transfer method", *Geomech. Eng.*, **20**(4), 359-370. https://doi.org/10.12989/gae.2020.20.4.359.

Cui, M.Z., Ren, W.X. and Yin, Y.G. (2021), "Numerical analysis and field load testing of a suspension bridge with a root pile anchorage", *Structures*, **34**, 1373-1382. https://doi.org/10.1016/j.istruc.2021.08.086.

D 'Appolonia, E. and Romualdi, J.P. (1963), "Load transfer in end-bearing steel H-piles", *ASCE Soil Mech. Found. Div. J.*, **89**(2), 11-25. https://doi.org/10.1061/JSFEAQ.0000496.

Ding, H., Su, L.J., Lai, J.X. and Zhang, Y.H. (2017), "Development and prospect of root Piles in tunnel foundation reinforcement", *Civ. Eng. J.Staveb. Obz.*, **26**(3). https://doi.org/10.14311/CEJ.2017.03.0022.

Dias, T.G.S. and Bezuijen, A. (2018), "Load-transfer method for piles under axial loading and unloading", *J. Geotech. Geoenviron.*, **144**(1), 1-9. https://doi.org/10.1061/(ASCE)GT.1943-5606.0001808.

Fan, Z.H., Wang, Y.H., Xiao, H.B. and Zhang, C.S. (2007), "Analytical method of load-transfer of single pile under expansive soil swelling", *J. Cent. South Univ. T*, **14**(4), 575-579. https://doi.org/10.1007/s11771-007-0110-4.

Huang, M.S., Zhang, C.R., Mu, L.L. and Gong, W.M. (2011), "Analysis of anchor foundation with root caissons loaded in nonhomogeneous soils", *Can Geotech. J.*, **48**(2), 234-246. https://doi.org/10.1139/T10-046.

JGJ 94-2008 (2008), Technical code for building pile foundations, *China Architecture Press*, Beijing, China.

JGJ 106-2014 (2014), Technical code for testing of building foundation piles. China Architecture Press, Beijing, China.

Kulhawy, F.H., Kozera, D.W. and Withiam, J.L. (1979), "Uplift testing of model drilled shafts in sand", *J. Geotech. Eng. Div. - ASCE*, **105**(1), 31-47. https://doi.org/10.1061/AJGEB6.000075.

Kong, G.Q., Yang, Q., Liu, H.L. and Liang, R.Y. (2013), "Numerical study of a new belled wedge pile type under different loading modes", *Eur. J. Environ. Civ. En.*, **17**, 65-82. https://doi.org/10.1080/19648189.2013.834586.

Liu, J.W., Guo, Z. and Han, B. (2019), "Load transfer of offshore open-ended pipe piles considering the effect of soil plugging", *J. Mar. Sci. Eng.*, **7**(9), 1-19. https://doi.org/10.3390/jmse7090313.

Liu, X.R., Zhuang, Y., Zhou, X.H., Li, C., Lin, B.B., Liang, N.H., Zhong, Z.L. and Deng, Z.Y. (2023), "Numerical study of the mechanical process of long-distance replacement of the definitive lining in severely damaged highway tunnels", *Undergr. Sp.*, **9**, 200-217. https://doi.org/10.1016/j.undsp.2022.07.007.

Luo, X.G., Ren, W.X., Yin, Y.G. and Yu, Y.C. (2022), "A modified hyperbolicity-based load transfer model for nonlinear settlement analysis of root piles in multilayered soils", *Acta Geotech.*, **17**(1), 303-317. https://doi.org/10.1007/s11440-021-01215-8.

Moayedi, H. and Mosallanezhad, M. (2017), "Uplift resistance of belled and multi-belled piles in loose sand", *Measurement*, **109**, 346-353. https://doi.org/10.1016/j.measurement.2017.06.001.

O'Neill, M.W. (2001), "Side resistance in piles and drilled shafts", *J. Geotech. Geoenviron.*, **127**(1), 3-16. https://doi.org/10.1061/(ASCE)1090-0241(2001)127:1(3).

Qian, Z.Z., Lu, X.L. and Yang, W.Z. (2019), "Comparative field tests on straight-sided and belled piers on sloping ground under combined uplift and lateral loads", *J. Geotech. Geoenviron.*, **145**(1), 1-14. https://doi.org/10.1061/(ASCE)GT.1943-5606.00019.

Randolph, M.F. and Wroth, C.P. (1978), "Analysis of the deformation of vertically loaded piles", *J. Geotech. Eng. Div. - ASCE*, **104**(12), 1465-1488.

Reddy, E.S.B., Oreilly, M. and Chapman, D. (1997) "A software to predict the behaviour of tension piles", *Comput. Struct.*, **62**(4), 653-658. https://doi.org/10.1016/S0045-7949(97)80002-3.

Rattley, M.J., Richards, D.J. and Lehane, B.M. (2008), "Uplift performance of transmission tower foundations embedded in clay", *J. Geotech. Geoenviron.*, **134**(4), 531-540. https://doi.org/10.1061/(ASCE)1090-0241(2008)134:4(531).

Seed, H.B. and Reese, L.C. (1957), "The action of soft clay along friction piles", *Transactions of the Am. Soc. Civil Engineers*, **122**, 731-754.

Wang, R. (2013), "Derivation and revision of the theoretical formula of friction stress between pile and soil on space axisymmetric condition considering relative slip", *Appl. Mech. Mater.*, **405-408**, 237-242. https://doi.org/10.4028/www.scientific.net/AMM.405-408.237.

Wang, Q.K., Hu, Z.B., Ji, Y.K., Ma, J.L. and Chen, W.L. (2022), "Centrifugal model test based bearing characteristics and analytical model of uplift pile in combined composite ground", *Rock Mech. Rock Eng.*, **55**(6), 3525-3543. https://doi.org/10.1007/s00603-022-02820-z.

Xu, C.J., Ding, H.B., Luo, W.J., Tong, L., Chen, Q.S. and Deng, J.L. (2020), "Experimental and numerical study on performance of long-short combined retaining piles", *Geomech. Eng.*, **20**(3), 255-265. https://doi.org/10.12989/gae.2020.20.3.255.

Yao, W.J., Chen, S.P. and Zhu, S.Q. (2012), "Elasto-plastic analysis method for vertically loaded pile considering pile-soil slip", *Appl. Mech. Mater.*, **105-107**, 1567-1571.
https://doi.org/10.4028/www.scientific.net/AMM.105-107.1567.

Yu, M.Y., Liu, B.G., Wang, Q. and Song, Y. (2020), "Study on bearing capacity of belled uplift piles in soft clay area", *Indian Geotech. J.*, **50**(5), 848-858. https://doi.org/10.1007/s40098-020-00420-8.

Zhang, S.G., Yuan, Z.R. and Sun, C.H. (2013), "Nonlinear analysis of deformation for belled tension piles under vertical loading", *Chinese J. Geotech. Eng.*, **35**(2), 1091-1094. (in Chinese)

Zhou, J.P., Huang, X.F., Zhang, J.L., Wei, L.H. and Yuan, J. (2021), "Experimental investigation of the uplift and lateral bearing capacity of root piles", *Soil. Mech. Found. Eng.*, **57**(6), 473-479. https://doi.org/10.1007/s11204-021-09695-2.

CC